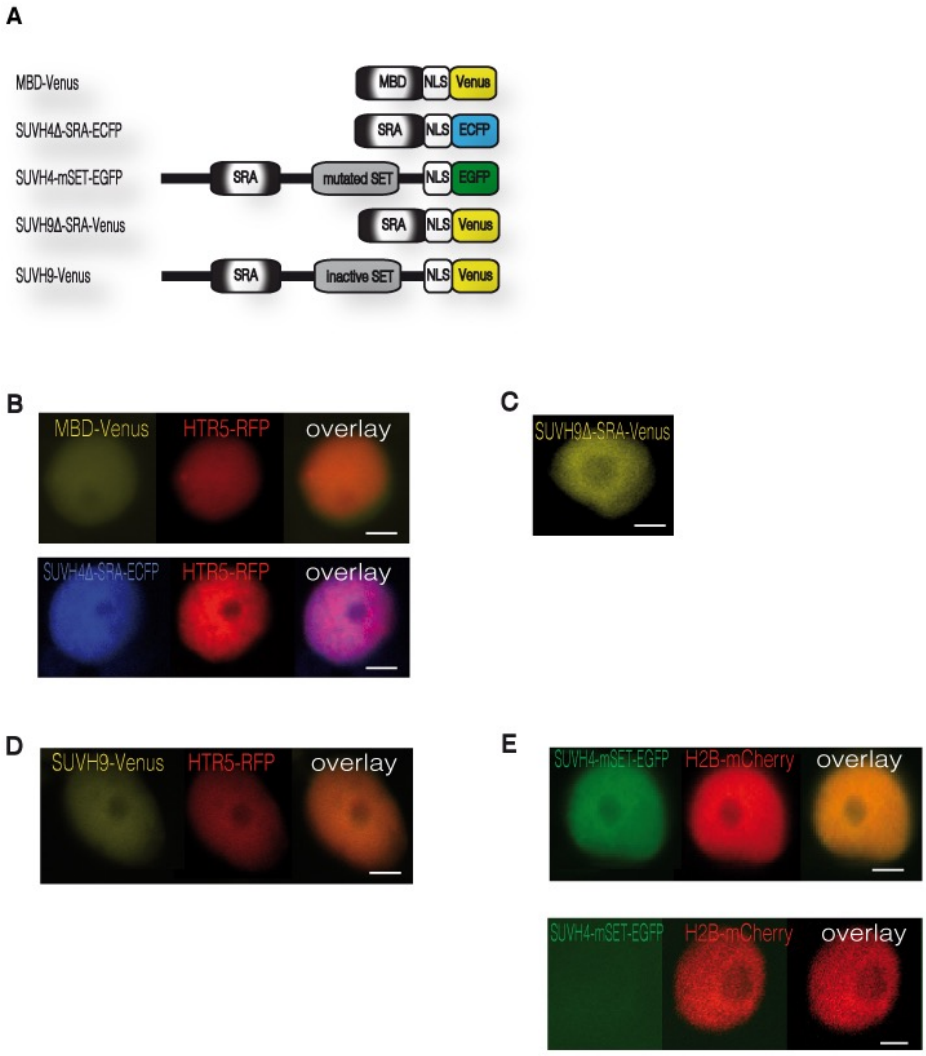

Supplemental Fig. 1. Transient expression of dynamic reporters of DNA methylation (DYNAMETs) in plants.

(A) Schematic representation of potential dynamic reporter of DNA methylation (DYNAMET). A DYNAMET contains a domain/protein binding methylated cytosines (mC) fused to a nuclear localization signal (NLS) in frame with a fluorescent protein (ECFP, EGFP, Venus variant of YFP). The region targeting mC corresponds to the methyl-binding domain (MBD) of MBD6, the SRA domain of SUVH4 (SUVH4*Δ*-SRA) or SUVH9 (SUVH9*Δ*-SRA). Representations are not drawn to scale. *(B)* Confocal images of transiently co-expressed DYNAMETs with a chromatin marker encoding a histone variant H3.3 fused to RFP (HTR5-RFP) in *Nicotiana benthamiana* leaf epidermal cells. *(C)* Confocal image of tobacco leaves infiltrated with a construct harboring SUVH9Δ-SRA-Venus. *(D)* Confocal images of transiently co-expressed SUVH9-Venus with a chromatin marker encoding a histone variant H3.3 fused to RFP (HTR5-RFP) in *Nicotiana benthamiana* leaf epidermal cells. *(E)* Representative confocal images of SUVH4-mSET-GFP in transiently transformed tobacco leaf nucleus (top panel) and stable transgenic Arabidopsis plants (leaf nucleus, bottom panel). Plants were transformed with the binary vector pMI108 containing two expression cassettes pHTR5:SUVH4-mSET-EGFP; pHTR5:H2B-mCherry in the same T-DNA. Bars, 2 μm.

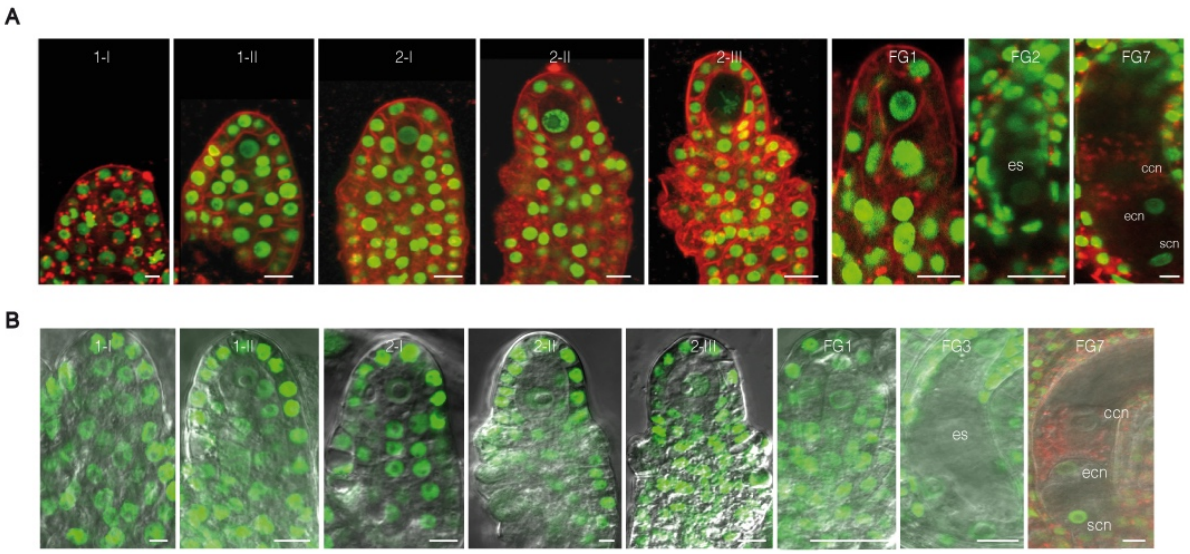

Supplemental Fig. S2. Activity of the *HISTONE THREE RELATED 5* (*HTR5*) promoter during female sporogenesis and gametogenesis.

Confocal images were generated from transgenic plants expressing *pHTR5:HTR5-GFP (A)* or *pHTR5:NLS-GUS-GFP*. *(B)* Fluorescence is detected in all cell types during female sporogenesis from stages 1-I to 2-III and female gametogenesis from stage FG1 to FG7. One exception is observed in the mature female gametophyte (stage FG7) where no fluorescence is detected in the central cell nucleus (ccn). Bars, 5 µm. Abbreviations: ecn, egg cell nucleus; es, embryo sac; scn, synergid cell nucleus. n> 15 observations for each stage. Bars, 5 µm.

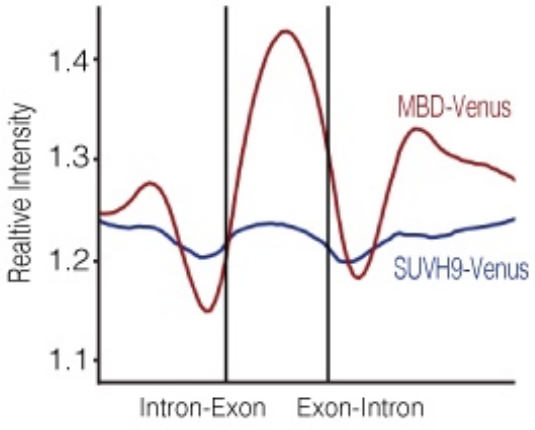

Supplemental Fig. S3. Distribution of MBD-Venus and SUVH9-Venus protein binding intensities across exons and introns.

Aggregate profiles obtained from ChIP-seq analyses were calculated from the complete set of Arabidopsis predicted genes in TAIR10. Consistent with published genome-wide methylome analyses (Cokus et al. 2008; Lister et al. 2008), MBD-Venus is enriched at exons relative to introns, in contrast to SUVH9-Venus that remains at a background level.

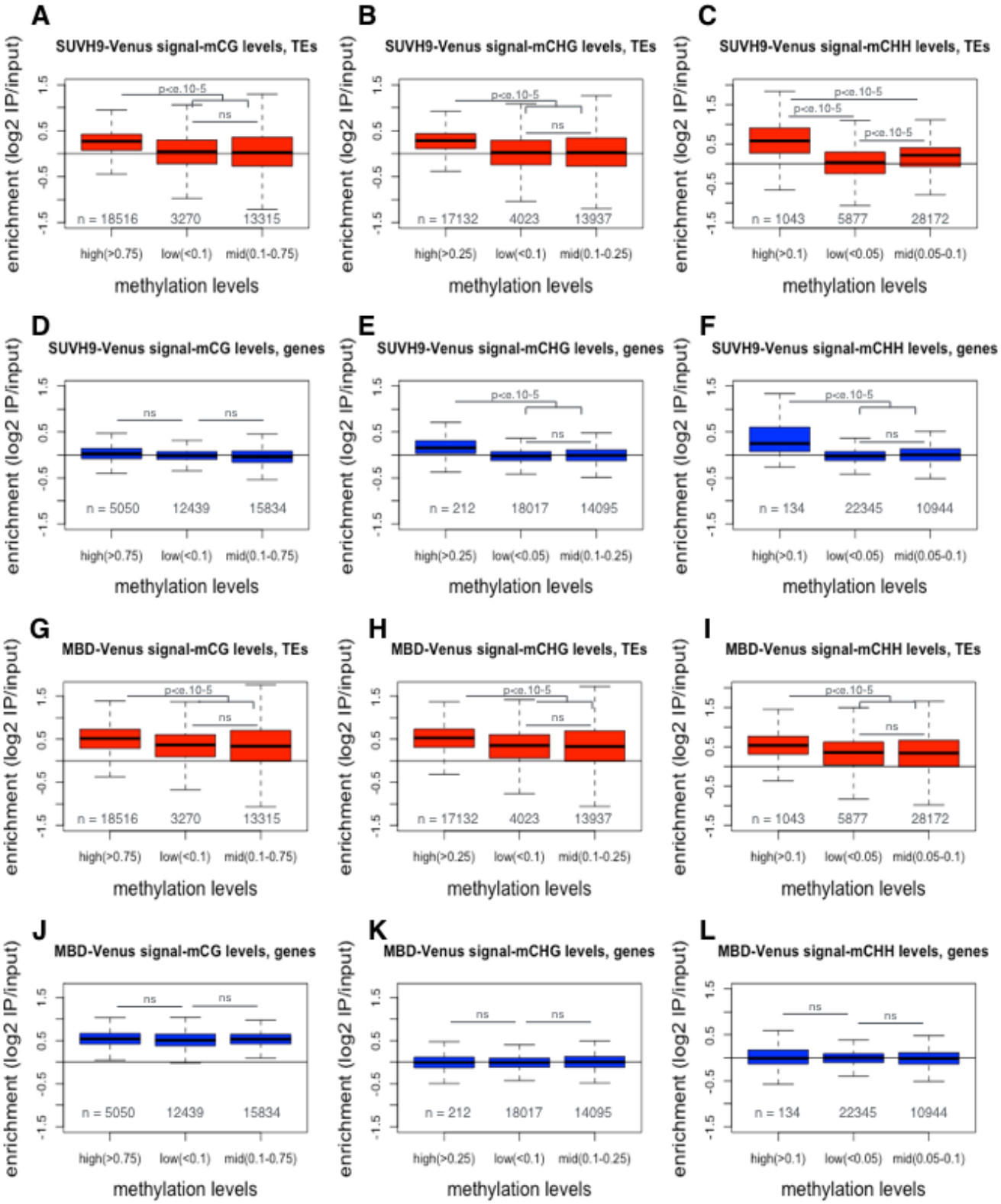

Supplemental Fig. S4 Boxplots of MBD-Venus and SUVH9-Venus enrichment relative to the three contexts of cytosine methylation in genes and transposable elements (TEs). *(A-C)* SUVH9-Venus enrichment in TEs for mCG, mCHG and mCHH. *(D-F)* SUVH9-Venus enrichment in genes for mCG, mCHG and mCHH. *(G-I)* MBD-Venus enrichment in TEs for mCG, mCHG and mCHH.*(J-L)* MBD-Venus enrichment in genes for mCG, mCHG and mCHH.

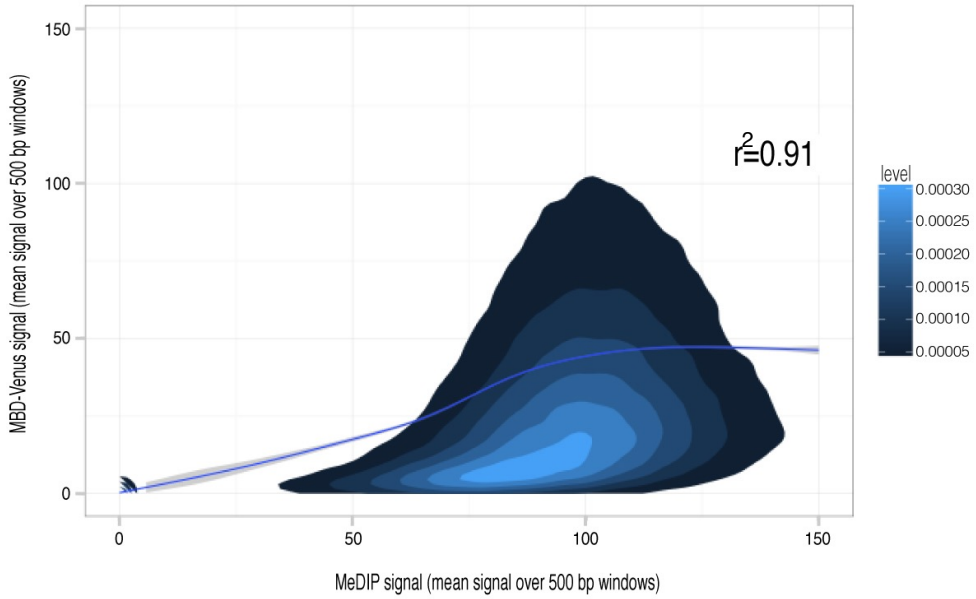

Supplemental Fig. S5. Correlation between MBD-Venus ChIP-seq and MeDIP-seq data.

Mean signal over 500 bp window for MeDIP (X axis) and MBD-Venus (Y axis). Color coding is used to display over-plotted areas (lighter blue representing the highest density of over-plotting).

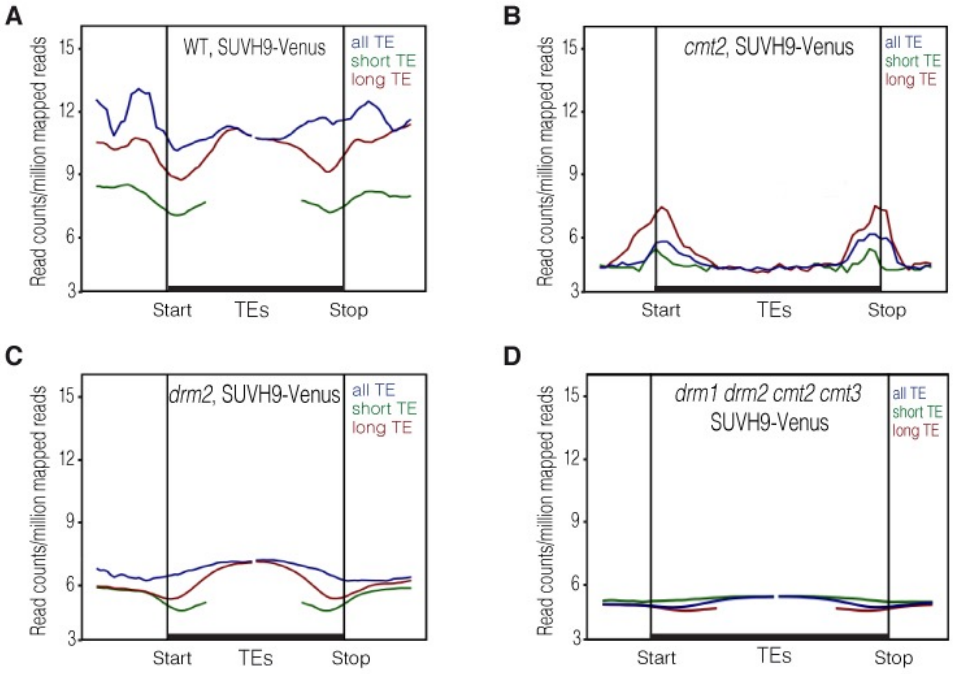

Supplemental Fig. S6. Distribution of SUVH9-Venus in the WT and in mutants affected in DNA methylation.

Average distribution of SUVH9-Venus protein binding intensities over transposable elements (TEs) in WT *(A)*, *drm2 (B), cmt2 (C)* and *drm1drm2cmt2cmt3 (D)* plants.

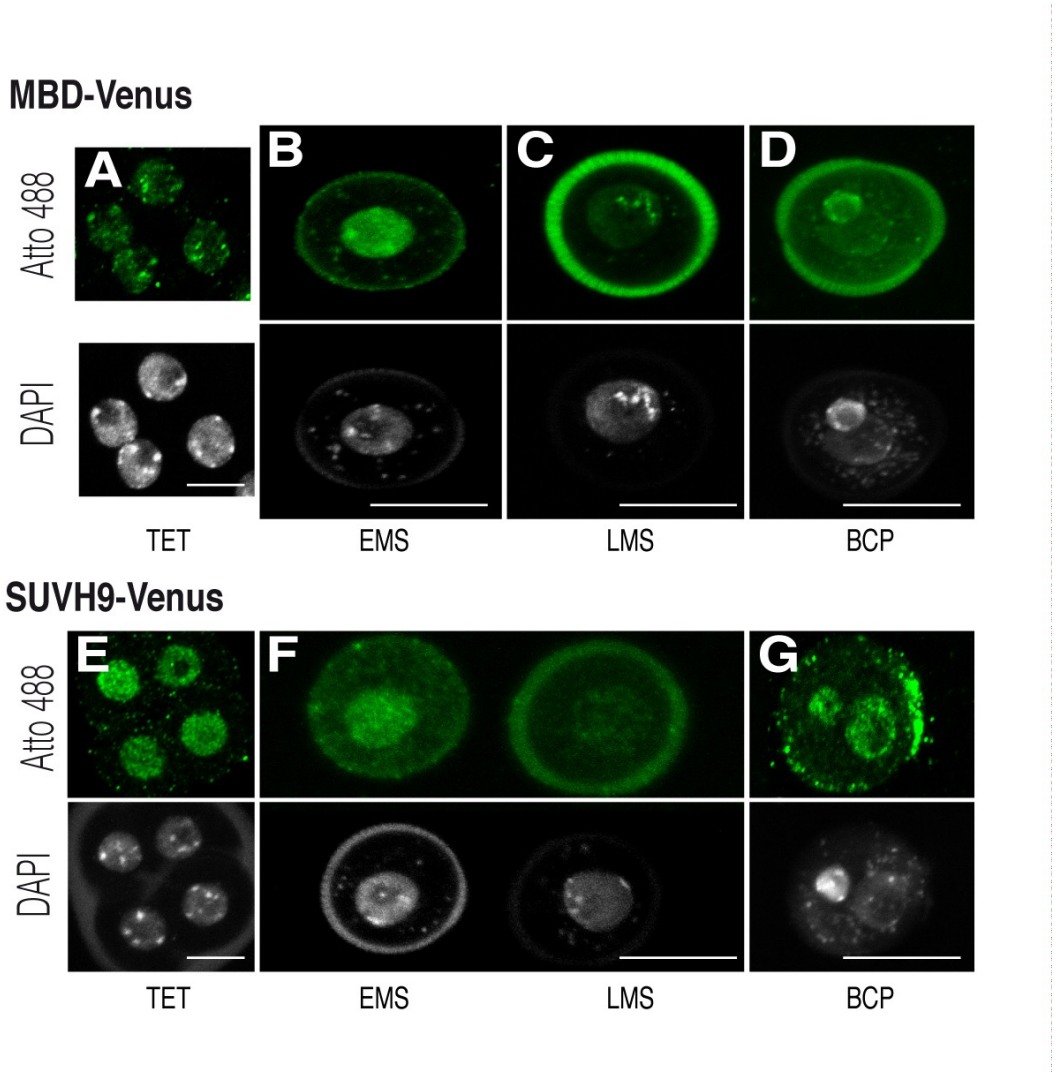

Supplemental Fig. S7. Nuclear pattern of MBD-Venus and SUVH9-Venus during male gametogenesis.

Representative confocal images of differentiating male gametophytes immunostained with an Atto 488-conjugated anti-GFP antibody and counterstained with DAPI. *(A,E)* Tetrads (TET) of haploid microspores, microspores before *(EMS, B,F left)* and after *(LMS, C,F right)* exine accumulation, Bicellular pollen grains (BCP) with a large vegetative cell and a smaller generative cell *(D,G)*. Bar, 10 µm *(A,E)* and 20 µm *(F-G)*. Number of observations for each stage, n> 25.

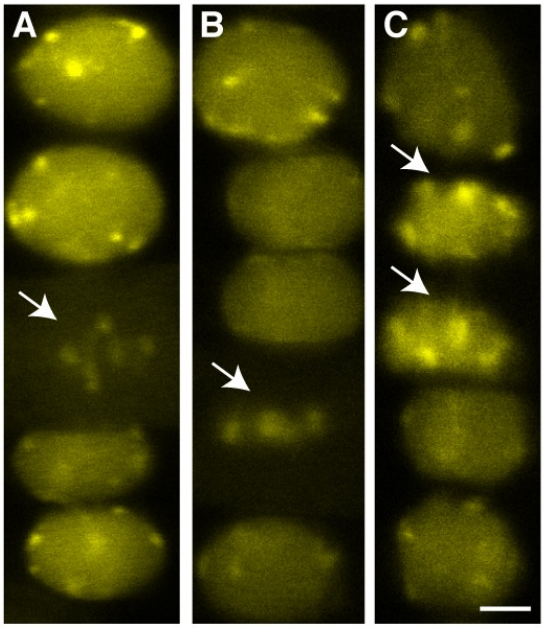

Supplemental Fig. S8. Dynamics of mCG-Venus in diving root cells.

Dynamics of mCG-Venus during mitosis in roots by confocal microscopy. *(A)* metaphase**,** *(B)* anaphase, *(C)* late telophase. Bar, 5 μm.

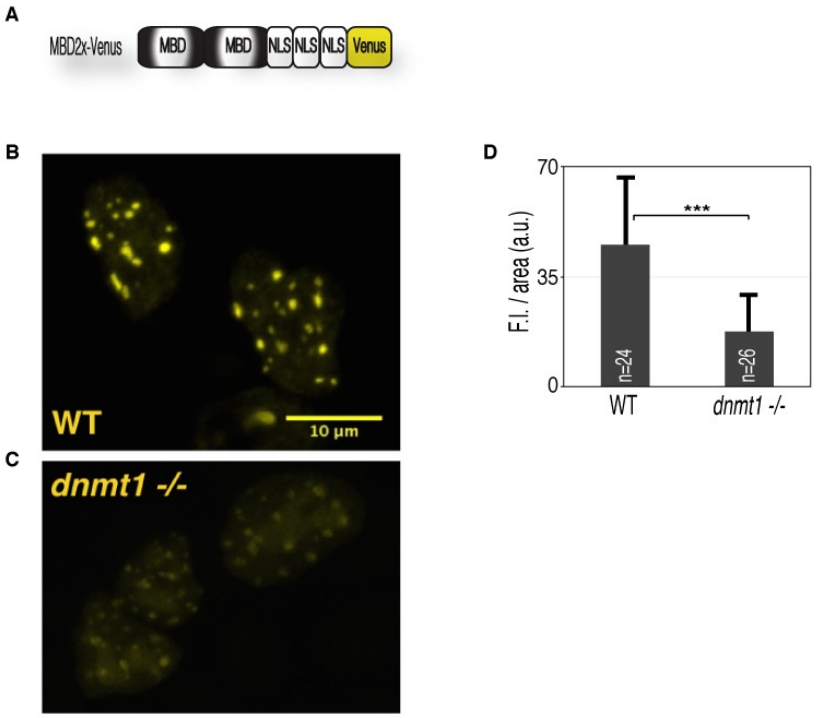

Supplemental Fig. S9. Distribution of MBD2x-Venus reporter in wild type and *dnmt1* knock-out living mouse embryonic stem cells.

(A) Schematic representation of MBD2x-Venus construct. The region targeting methylated cytosine corresponds to the methyl-binding domain (MBD) of MBD6 of Arabidopsis arranged in tandem fused to a triple nuclear localization signal (NLS) and a yellow fluorescent protein (Venus). Representation is not drawn to scale. Subcellular distribution of MBD2x-Venus in the wild type *(B)* and *dnmt1* knock out *(C)* ESCs, under identical illumination settings. Bar, 10 µm. *(D)* Relative fluorescence intensity (F.I) of MBD2x-Venus in wild type and *dnmt1 -/-* ESCs. a.u, arbitrary units. ***, $p<0.002$.

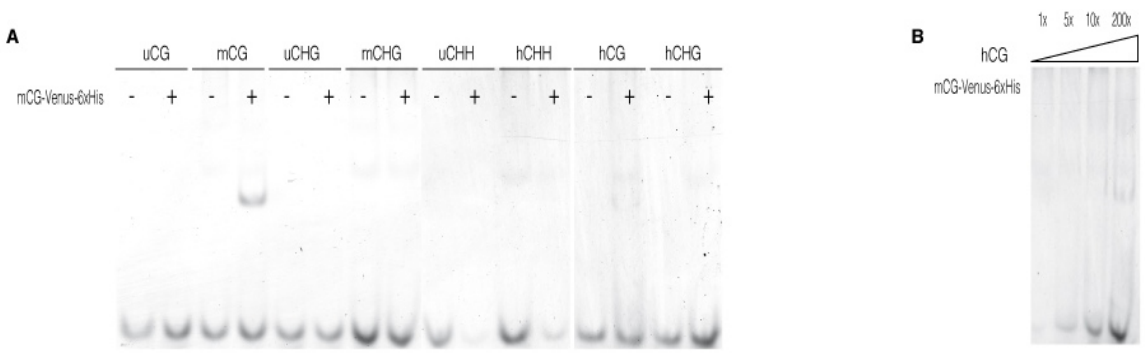

Supplemental Fig. S10. mCG-Venus binds specifically to symmetric DNA methylation in the CG sequence context.

Electrophoretic mobility shift assay with purified mCG-Venus-6xHis protein and FAM-labeled dsDNA oligonucleotides either unmethylated (u), hemimethylated (h) or fully methylated (m) in the CG, CHG and CHH sequence context (H can be either A, T or C).

(A) Binding of mCG-Venus-6xHis to unmethylated (u), hemimethylated (h) or fully methylated (m) cytosines in different sequence contexts.

(B) Binding of mCG-Venus-6xHis to increasing concentration of hemi-methylated cytosines in the CG sequence context (hCG).

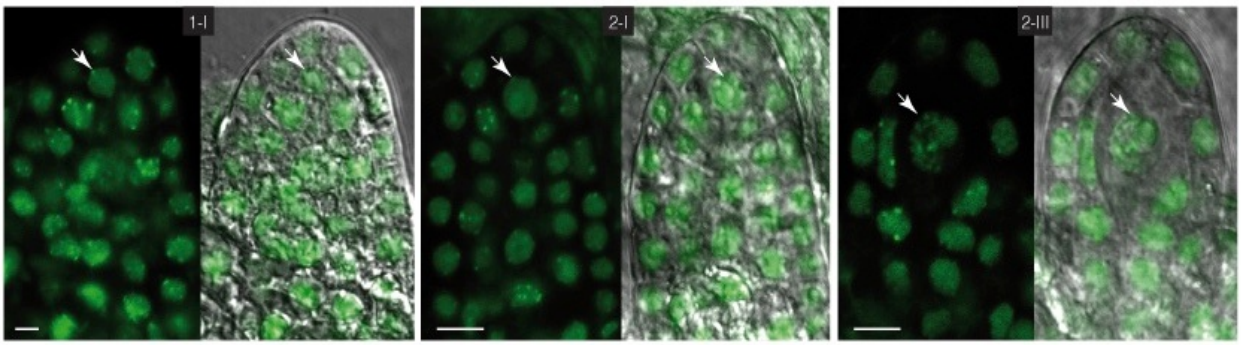

Supplemental Fig. S11. Chromatin structure at chromocenters during female sporogenesis.
To evaluate chromatin structure at chromocenters during female sporogenesis, we analyzed the nuclear pattern of a polydactyl zinc finger reporter line targeting the 180-bp repeats (Lindhout et al. 2007). At all stages of female sporogenesis (stage 1 to stage 2), fluorescent heterochromatin foci are visible in the developing megaspore mother cell (arrow). Outline of developing female spores are provided by DIC images. n> 10 observations per stage. Bars, 5 µm.

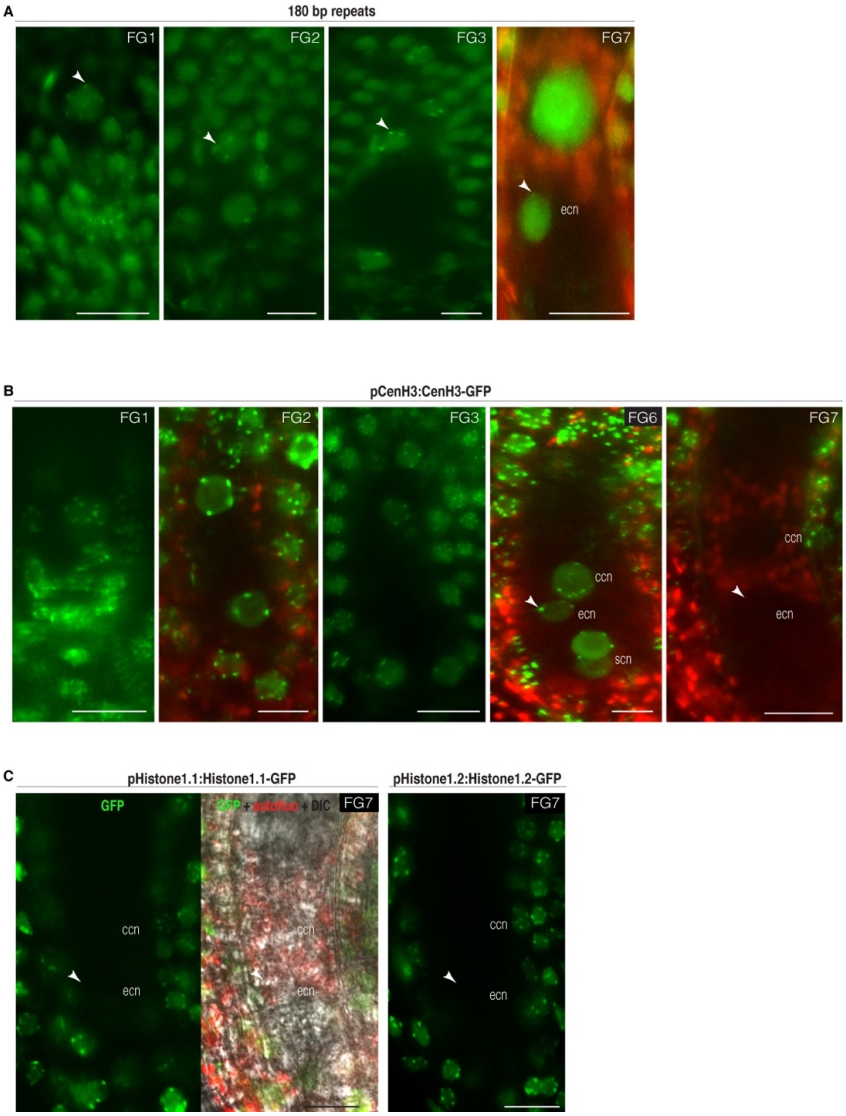

Supplemental Fig. S12. Chromatin structural changes at chromocenters during female gametogenesis.

(A) Pattern of a 180-bp repeats reporter (Lindhout et al. 2007). Dense heterochromatin foci corresponding to tagged 180-bp repeats are observed in each haploid nucleus of the proliferating female gametophyte (FG, arrow). In the mature FG (stage FG7) these foci become more discrete in the egg cell nucleus suggesting a more relaxed constitutive heterochromatin. Bars, 40 µm for FG1, FG2, FG3 and 20 µm for FG7. *(B)* Dynamics of tagged centromeric H3 histone (CenH3) variant (Fang and Spector 2007). Five foci corresponding to centromeres are detected in each haploid nucleus of the proliferating female gametophyte (FG1 to FG3). Foci are detected in all cell types of the FG until the stage FG6. In the mature ovule (stage FG7), CenH3-GFP becomes undetectable. Bars, 40 µm for FG1, FG2, FG3 and 20 µm for FG6 and FG7. *(C)* Dynamics of two linker H1 histones (H1.1 and H1.2) tagged with a GFP (She et al. 2013) in the mature ovules. Although both tagged linker histones accumulate at the heterochromatin foci in somatic cells, no fluorescence can be detected in the two female gametes, the egg cell and central cell. n> 20 observations per stage. Bars, 20 µm.

Fluorescent images are combined with differential interference contrast (DIC) and autofluorescence (red) that labels the central cell. Abbreviations: ccn, central cell nucleus; ecn, egg cell nucleus; scn, synergid cell nucleus.

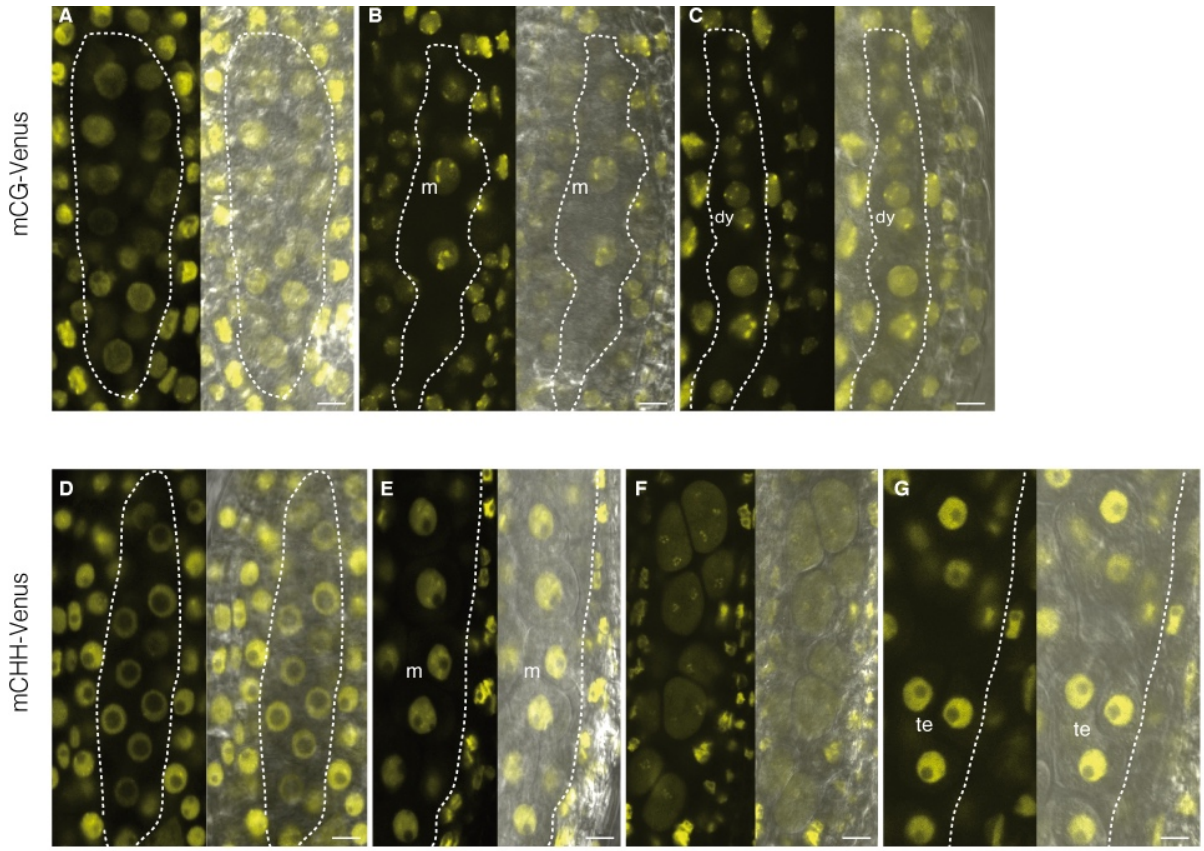

Supplemental Fig. S13. Dynamics of DYNAMETs reporters during pollen mother cell differentiation and male meiosis.

Dynamics of mCG-Venus *(A-C)* and mCHH-Venus *(D-G)* fluorescence from pollen mother cell (PMC) differentiation *(A,B,D,E)* until formation of the dyad *(C)* and the tetrad *(G)* after meiosis. Contours of the anther locules containing developing and dividing PMC are marked by a dotted line. For each stage, a confocal image is combined with differential interference contrast (DIC) image. n> 10 observations per stage. Bars 5 µm. Abbreviations: dy, dyad; m, meiocyte; te, tetrad.

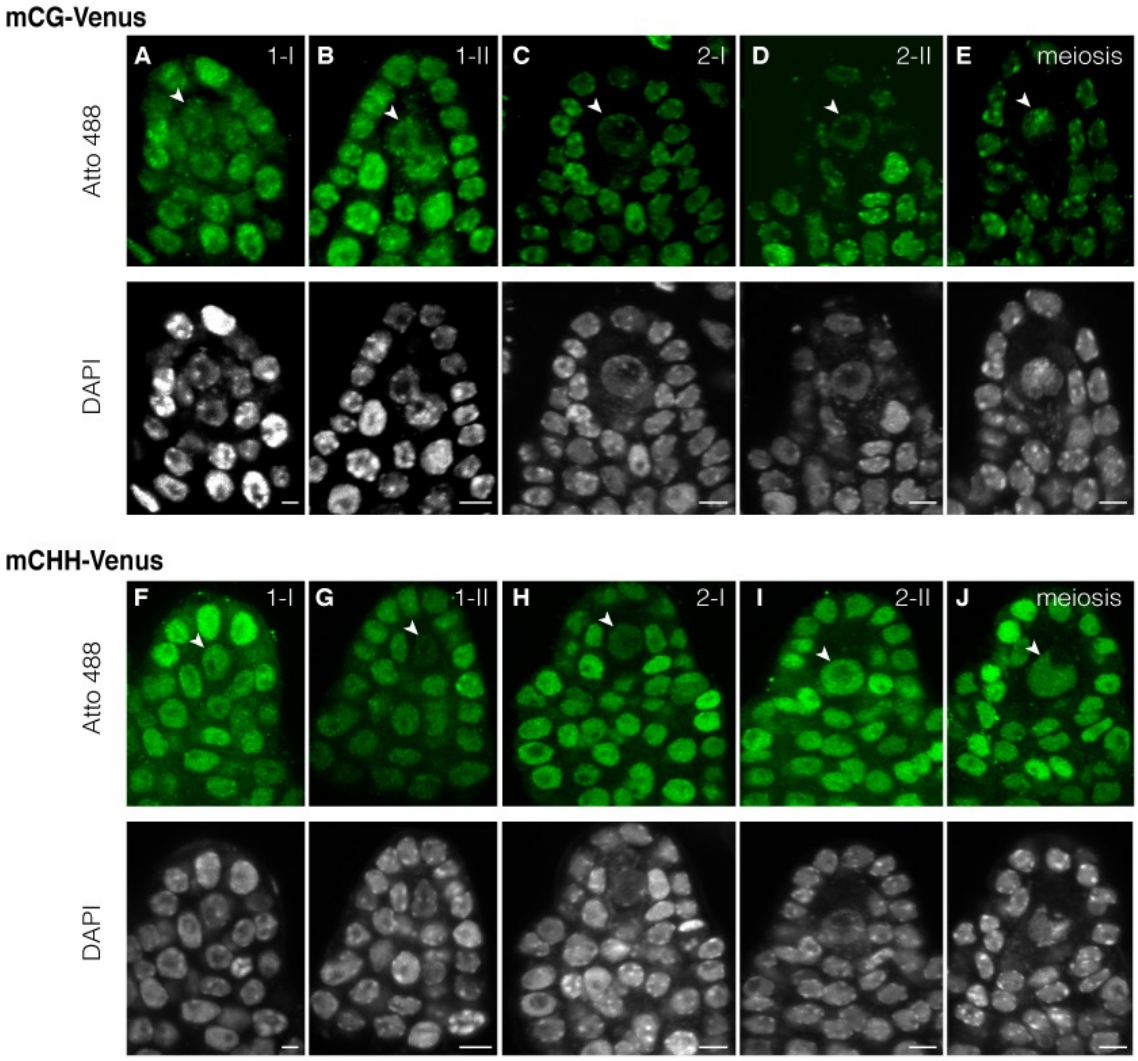

Supplemental Fig. S14. Nuclear pattern of mCG-Venus and mCHH-Venus during female sporogenesis.

Representative confocal images of differentiating megaspore mother cells (from stage 1-I to 2-II, arrow) and undergoing meiosis (arrow) immunostained with an Atto 488-conjugated anti-GFP antibody and counterstained with DAPI. n> 20 observations per stage. Bar, 5 μm.

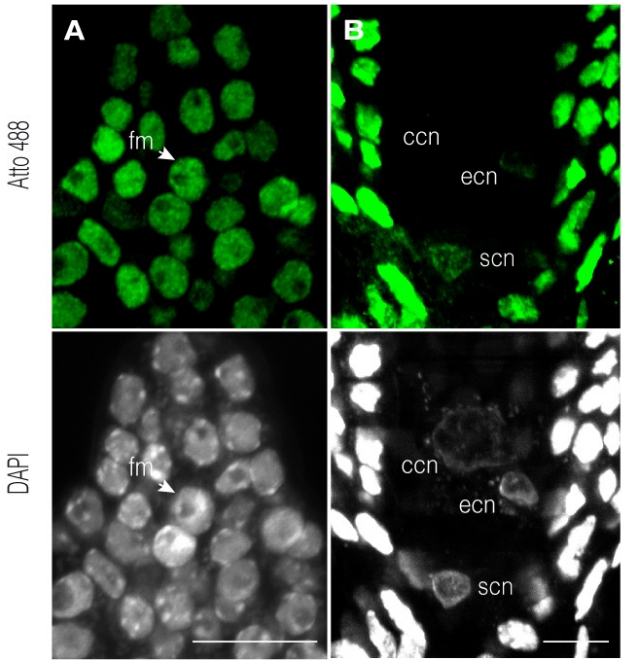

Supplemental Fig. S15 Nuclear pattern of mCG-Venus in the female gametophyte.

Representative confocal images of immunostained female gametophytes with an Atto 488-conjugated anti-GFP antibody and counterstained with DAPI. Female gametophyte at stage FG1 *(A)* and FG7 *(B)*. Abbreviations: fm, functional megaspore; ecn, egg cell nucleus; ccn, central cell nucleus; syn, synergid cell nucleus. n> 20 observations per stage. Bars, 10 µm for *(A)* and 15 µm for *(B)*.

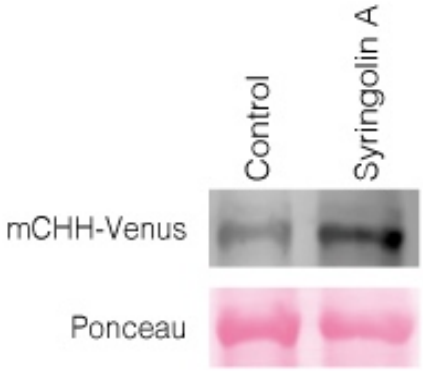

Supplemental Fig. S16. mCHH-Venus is targeted for proteasome-dependent degradation.
Flower buds from transgenic plants expressing mCHH-Venus were incubated during 18 h in ½ MS medium with or without a proteasome inhibitor syringolin A (5 µM). Total protein extracts from mCHH-Venus were subjected to immunoblot assays using an anti-GFP antibody. Equal protein loading was assessed after Ponceau staining.

A

Genetic Cross	Abnormal F1 embryos %	n	rep.
Col x Col	4.8 (+/-0.9)	687	12
drm2-2 x *drm2-2*	14.9 (+/-1.7)***	323	4
drm2-2 x Col	11.7 (+/-2.3)***	655	13
Col x *drm2-2*	9.9 (+/-1.3)**	252	3
drm2-2/+ x Col	12.9 (+/-3.1)**	147	3

B

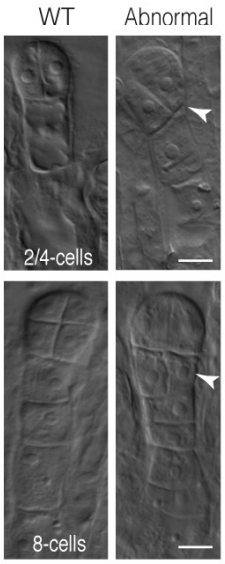

Supplemental Fig. S17. Loss of maternal DRM2 function results in abnormal early embryo patterning.

(A) Percentage of embryos with cell division planes defects among total seeds (n) from zygote to 16 cells stage. Results are presented as the mean percentage (+/- SE) of several independent rounds of crosses and observations (rep). The p value for a Two-Tailed Fisher's exact test comparing percentage of abnormal embryos observed in each cross respective to the wild type cross is indicated. ***, $p<0.001$; **, $p<0.01$. *(B)* Representative abnormal embryo phenotypes showing aberrant divisions (arrow) in either the embryo proper or the suspensor domain. Bars, 10 µm.

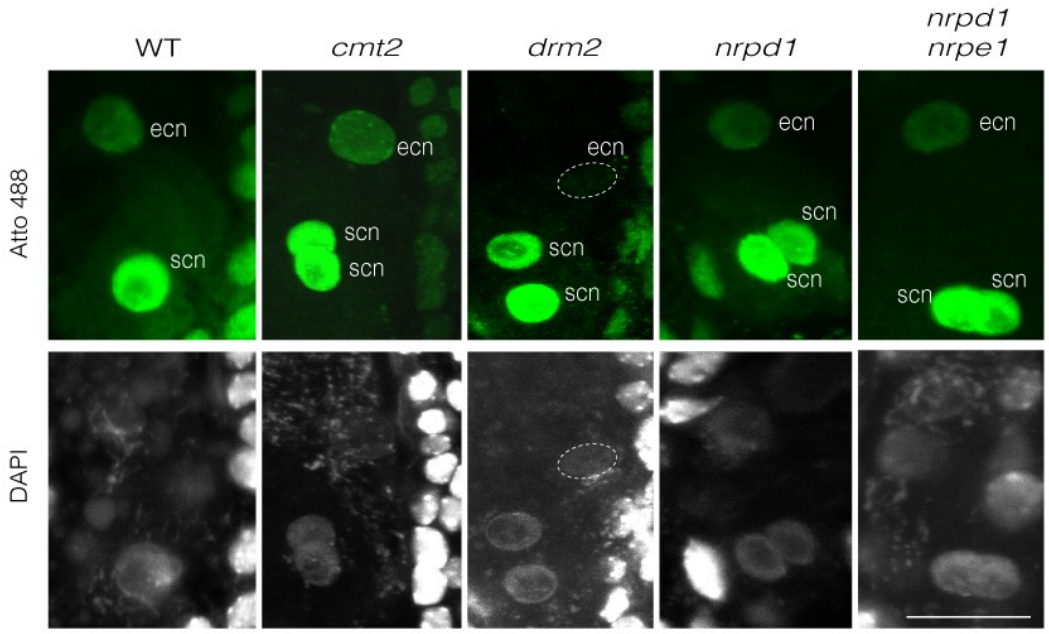

Supplemental Fig. S18 Nuclear pattern of mCHH-Venus in the egg cell in the wild type and mutants affected in cytosine methylation. Representative confocal images of mature female gametophytes immunostained with an Atto 488-conjugated anti-GFP antibody and counterstained with DAPI. Bar, 5 μm.

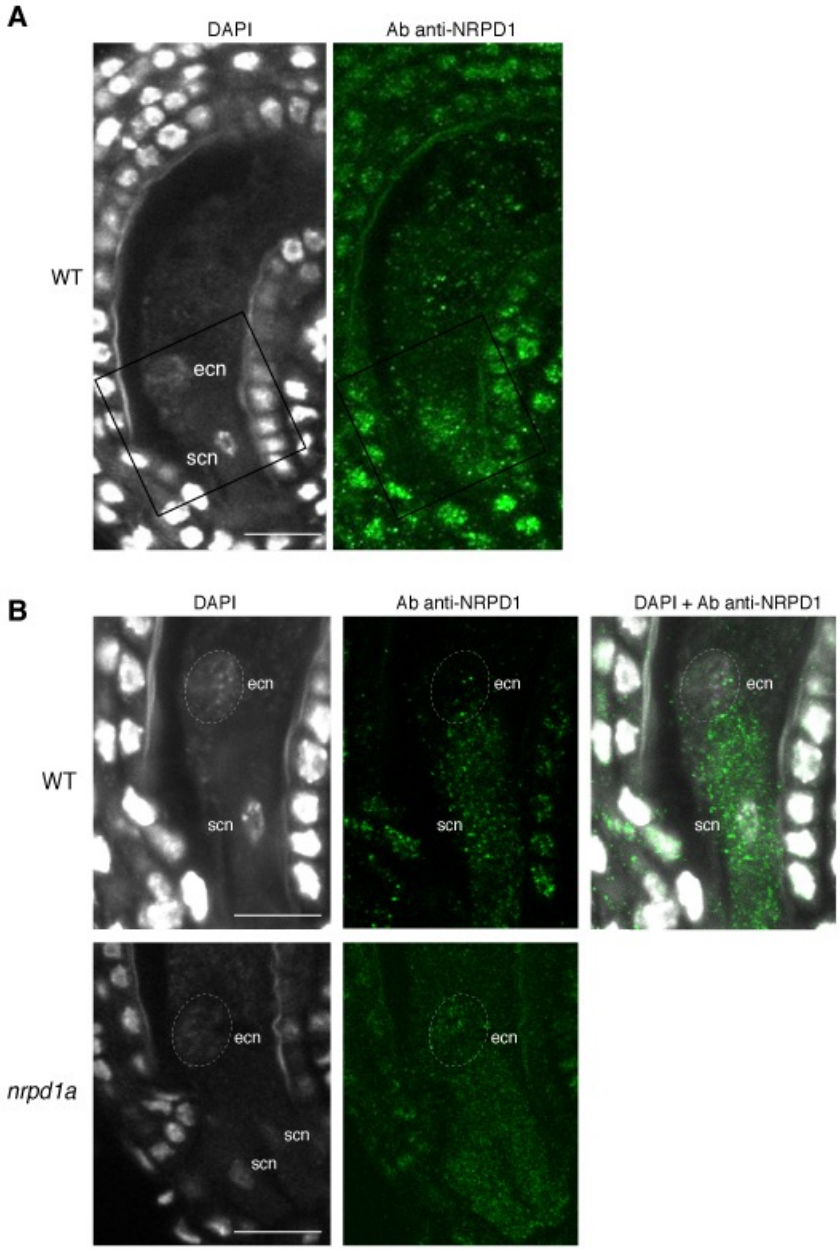

Supplemental Fig. S19. Immulocalization of NRPD1 in mature female gametophytes of WT and *nrpd1* mutant plants.

(A) Whole view of the female gametophyte for DAPI (left) and NRPD1 (right). The nuclear pattern is consistent with previously published patterns in somatic nuclei (Haag et al. 2009). *(B)* Close-up of the egg apparatus. A strong signal is detected in the synergids in the WT that is reduced to background level in the null mutant for *NRPD1*. Number of observations, n= 22, with 2 biological replicates. Abbreviations: ecn, egg cell nucleus; scn, synergid cell nucleus. Bars 20 µm.

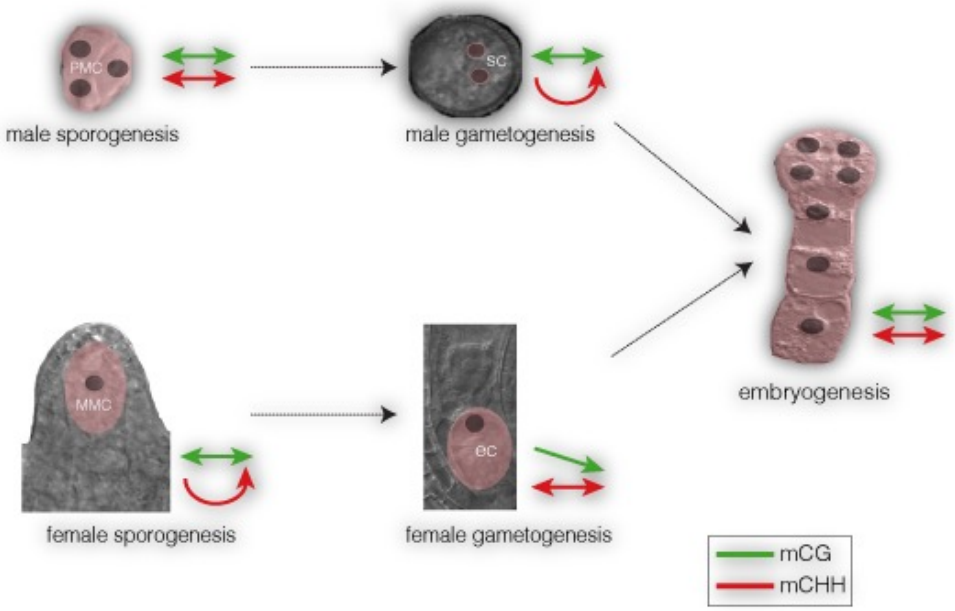

Supplemental Fig. S20. CG and CHH methylation dynamics during plant reproduction.
Dynamics of methylation patterns in CG and CHH sequences (where H can be A, T or C) as observed with the dynamic reporters of DNA methylation (DYNAMETs) during plant reproduction in Arabidopsis. Overall CG methylation pattern is stably maintained throughout male/female sporogenesis and gametogenesis indicating that CG methylation is not reprogrammed as typically encountered in mammals. CG methylation becomes transiently hemi-methylated in the egg cell (ec) at maturity due to lack of maintenance but symmetrical CG methylation is rapidly restored in the early embryo. In contrast CHH methylation is reprogrammed during male gametogenesis and female sporogenesis.
Abbreviations: MMC, megaspore mother cell, PMC, pollen mother cell; sc, sperm cells.

Supplemental Movie S1. Time-lapse movie of mCG-Venus during mitosis.

Images of a dividing root cell were taken at 2-min intervals. Numbers indicate the time from the first frame in minutes.

Supplemental Movie S2. Time-lapse movie of mCHH-Venus of developing microspores within an anther locule.

Numbers indicate the time from the first frame in minutes. Images were taken at 30-min intervals over 16 hours.

Supplemental Movie S3. Time-lapse movie of mCHH-Venus in developping male meiocytes within an anther locule.

Numbers indicate the time from the first frame in minutes. Images were taken at 30-min intervals over 15 hours.